JOURNAL OF CATALYSIS 116, 130–143 (1989)

Influence of Intercrystalline Mass Transfer on Catalytic Properties of Pt · H–ZSM-5 · Al_2O_3 Catalyst

VASANT R. CHOUDHARY[1] AND DEEPAK B. AKOLEKAR

Chemical Engineering Division, National Chemical Laboratory, Pune 411 008, India

Received November 30, 1987; revised October 5, 1988

Influence of intercrystalline (macropore) mass transfer on the catalytic activity and product selectivity in *o*-xylene isomerization, isooctane cracking, and methanol-to-aromatics conversion reactions on Pt · H–ZSM-5 · Al_2O_3 has been investigated by varying the catalyst particle size. Effect of poisoning of both the inter- and intracrystalline acid sites of the catalyst on its catalytic activity and selectivity has also been investigated. The effective intercrystalline diffusivity of the zeolite catalyst under reaction conditions has been determined by studying a first-order reaction cracking of isooctane (which does not penetrate the zeolite channels) using the catalyst of different particle sizes and determining the effectiveness factor of the catalyst. Both the activity and the selectivity of the catalyst in the above reactions are strongly influenced by the intercrystalline mass transfer. © 1989 Academic Press, Inc.

INTRODUCTION

ZSM-5 zeolites have gained tremendous importance as commercial catalysts in the methanol-to-hydrocarbon conversion processes (*1–3*) and also in a number of hydrocarbon alkylation and conversion processes for the manufacture of *p*-xylene, ethylbenzene, *p*-ethyltoluene, diethylbenzene, etc. (*3, 4*).

It is a common practice that when zeolites are used as catalysts, particularly, in packed-bed reactors, these are used in the form of pellets or extrudates which consists of zeolite crystallites bounded by a binder. Though, zeolite crystals are microporous, the pelletization or extrudation gives rise to the intercrystalline pore system having a large pore diameter. These intercrystalline pores are commonly called macropores. In the commercial zeolite catalyst, in order to minimize intracrystalline mass transfer resistance, small size (<1 μm) zeolite crystallites are employed. The diffusivities of reactants and products for intercrystalline mass transfer are very much higher than those for intracrystalline mass transfer bu the diffusion path for intercrystalline mas transfer is much larger [because of th larger particle size ($\geq$1.5 mm) of the zeolit catalyst] than that for the intracrystallin mass transfer. Therefore, the intercrystal line mass transfer resistance cannot be ne glected and it is obviously necessary t know the relative importance of the micro pore (intracrystalline) and macro- and me sopore (intercrystalline) diffusion resis tances. The importance of both the micro and the macropore diffusion in pelleted ze olite catalysts has been emphasized in th recent review by Palekar and Rajadhyaksh (*5*).

In the conversion of dimethyl ether to hy drocarbons on ZSM-5 at 600 K, Riekert an co-workers (*6, 7*) observed that the inter crystalline mass transfer affects catalyti activity and selectivity of the zeolite pellet when diam >2 mm are used, whereas, in tracrystalline mass transfer does not seen to be important with respect to catalytic ac tivity and selectivity of the zeolite at <60 K. It is, therefore, very interesting to inves tigate the influence of intercrystalline mas transfer on the catalytic activity and selec

[1] To whom all correspondence should be addressed.

0021-9517/89 $3.00
Copyright © 1989 by Academic Press, Inc.
All rights of reproduction in any form reserved.

TABLE 1

Properties of the Pt · H–ZSM-5 · Al_2O_3 Catalyst

Catalyst form	Extrudates (diam: 0.16 cm)
Catalyst composition	Pt (0.1 wt%), H–ZSM-5 (50 wt%), and Al_2O_3 (50 wt%)
Crystal size of the H–ZSM-5	0.2–0.3 μm
Si/Al ratio of the H–ZSM-5	70
Bulk density of the catalyst	0.62 g · cm^{-3}
Data obtained by specific gravity bottle methods	
Particle (extrudate) density	1.02 g · cm^{-3}
Macro- and mesopore volume [$V_{(macro\ and\ meso)}$]	0.57 $cm^3 \cdot g^{-1}$
Micropore volume [$V_{(micro)}$]	0.09 $cm^3 \cdot g^{-1}$ (by sorption of *n*-hexane)
	0.07 $cm^3 \cdot g^{-1}$ (by sorption of *p*-xylene)
Porosity (micro) [$\varepsilon_{(micro)}$]	0.09
Porosity (macro and meso) [$\varepsilon_{(macro\ and\ meso)}$]	0.58
Data obtained by mercury porosimetry	
Macropore volume [$V_{(macro)}$]	0.16 $cm^3 \cdot g^{-1}$
Mesopore volume [$V_{(meso)}$]	$\geq$0.37 $cm^3 \cdot g^{-1}$
Porosity (macropores) [$\varepsilon_{(macro)}$]	0.16
Av macropore radius [$r_{p(macro)}$]	0.1 μm
Av mesopore radius [$r_{p(meso)}$]	7.0 nm
Surface area of macro- and mesopores [$S_{(macro\ and\ meso)}$]	
$S_{(macro\ and\ meso)}$ (obtained by N_2 sorption)	112 $m^2 \cdot g^{-1}$
$S_{(macro\ and\ meso)}$ (obtained by Hg porosimeter)	130 $m^2 \cdot g^{-1}$

tivity of the ZSM-5 zeolite for a number of catalytic processes.

In the present investigation, the influence of intercrystalline mass transfer on the catalytic activity and selectivity in the methanol-to-aromatics conversion *o*-xylene isomerization, and isooctane cracking over Pt · H–ZSM-5 · Al_2O_3 catalyst has been investigated by carrying out the reactions on the catalyst of different particle sizes in a pulse microreactor. The effective macropore (or intercrystalline) diffusivity of isooctane (which does not penetrate the intracrystalline channels of the zeolite) in the catalyst under reaction conditions during the catalytic reaction has also been determined.

EXPERIMENTAL

The catalyst Pt · H–ZSM-5 · Al_2O_3 (0.1 wt% Pt, 50 · 0 wt% Al_2O_3) in the form of extrudates of diam 0.16 cm was provided by Dr. P. Ratnasamy (National Chemical Laboratory, Pune-8). The properties of the catalyst and the ZSM-5 zeolite used herein are given in Table 1.

The catalyst was calcined in static air at 773 K for 4 h. It was crushed to different particle sizes (from 0.16- to 0.018-cm size particles). Before measuring acidity and catalytic properties of the catalyst, it was treated *in situ* in a flow of hydrogen at 673 K for 1 h.

The micro- and meso/macropore volumes of the catalyst were determined by measuring the sorption of isooctane, which penetrates the macro- and mesopores (i.e., intercrystalline and interalumina particle voids and also voids in the alumina particles) but not the zeolite channels and *n*-hexane and *p*-xylene which penetrate freely in both the meso/macropores and the micropores (i.e., intracrystalline zeolite channels of the catalyst) in the evacuated catalyst extrudates at room temperature by using the specific gravity bottle method (*8, 9*).

The N_2 sorption/adsorption on the catalyst at liquid N_2 temperature (78 K) and N_2 concentration of 30 mol% (balance helium) was measured by dynamic adsorption/desorption method using a Quantasorb Unit (Quantachrome Corp.).

The total amount of N_2 adsorbed (on the walls of macropores) and sorbed (in the micropores of the zeolite crystals) in the catalyst was found to be 3.66 mmol · g^{-1}. Since the N_2 sorption capacity of the pure crystals of the ZSM-5 zeolite at 78 K and at $p/p_s = 0.3$ has been found to be 5.0 mmol · g^{-1}, the amount of N_2 sorbed in the micropores of the catalyst is estimated to be 2.5 mmol · g^{-1}. Therefore, the amount of N_2 adsorbed in the macro- and mesopores of the catalyst is estimated to be 1.16 mmol · g^{-1}. From this, the surface area of the macro- and mesopores is estimated to be about 112 $m^2 \cdot g^{-1}$.

The pore size distribution of the nonzeolite pores in the catalyst is measured by mercury porosimetry using a Autoscan-33 Porosimeter (Quantachrome Corp.) by varying the pressure in the porosimeter from 0.0 to 33,000 psig. The pore size distri-

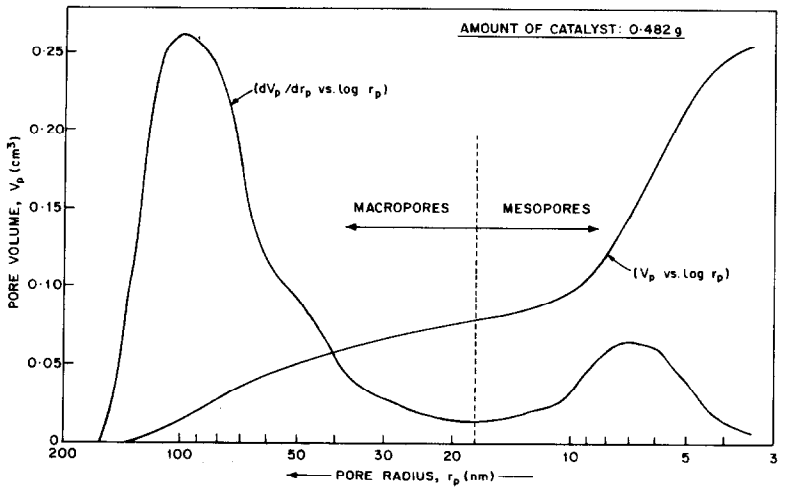

FIG. 1. Pore size distribution of the macro- and mesopores of the catalyst.

bution of the macro- and mesopores of the catalyst is presented in Fig. 1. The pore size distribution of the nonmicro (i.e., nonintracrystalline) pores is bimodal, indicating the presence of macropores (average diameter: 0.2 μm) and mesopores (average diameter: 14.0 nm). The data obtained from the porosimetry are included in Table 1.

The acid strength distribution of the catalyst was measured at near operating conditions by gas chromatographic adsorption/desorption methods: stepwise thermal desorption [STD] of pyridine (*11*) from 373 to 673 K and temperature-programmed desorption [TPD] of pyridine under chromatographic conditions (*11, 12*) from 373 to 673 K on the catalyst.

The catalytic reaction (viz. *o*-xylene isomerization, methanol-to-aromatics conversion, and isooctane cracking) on the catalyst of different particle sizes (0.018–0.16 cm) and also on the catalyst (particle size: 0.018 cm) poisoned with pyridine and/or 4-methylquinoline irreversibly chemisorbed at 623 K was carried out in a pulse microreactor (i.e.: 4 mm) connected to the gas chromatograph using hydrogen as a carrier gas. The details of the microreactor and procedures for carrying out the catalytic reactions and analyzing reaction products were given earlier (*13, 14*).

Selective poisoning of strong acid sites on the catalyst was carried out by saturating the catalyst with pyridine (or 4-methylquinoline) by its irreversible chemisorption at 623 K. The activity and selectivity of the poisoned catalyst in the *o*-xylene isomerization and isooctane cracking reactions were determined at 608 K. The detailed procedure for the selective poisoning is given elsewhere (*13, 15*).

Before carrying out the catalytic reactions or the catalyst poisoning, the catalyst was treated *in situ* with hydrogen (flow rate: 20 $cm^3 \cdot min^{-1}$) at 673 K for 1 h.

The adsorption equilibrium constant for isooctane on the catalyst was determined by the GC pulse technique (*16*).

RESULTS

Acidity Distribution

The acidity distribution of the catalyst has been measured by chemisorption/stepwise thermal desorption (STD) of pyridine and also by the TPD of pyridine under chromatographic conditions, at the temperatures close to those employed in the catalytic reactions.

Temperature dependence of the chemisorption of pyridine on the catalyst is shown in Fig. 2a. The site energy or acid

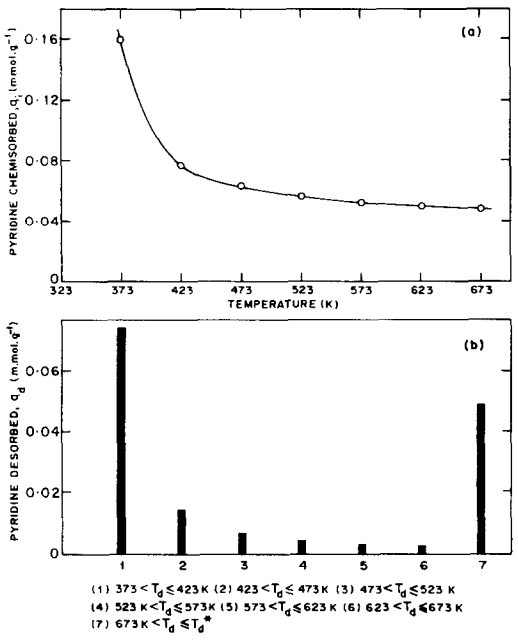

FIG. 2. (a) Temperature dependence of chemisorption of pyridine on the catalyst. (b) Acid strength distribution on the catalyst.

strength distribution obtained by the STD of pyridine on the catalyst is presented in Fig. 2b.

The TPD chromatograms on the catalyst at different initial concentrations (θ_i) of pyridine are shown in Fig. 3.

The TPD chromatograms have the following common features:

(a) The TPD curves are asymmetric and broad.

(b) The desorption edges of the superimposed TPD chromatograms (obtained at the different values of θ_i) lie on the common desorption curve.

(c) The start of desorption of pyridine is very sharp.

(d) The temperature at which desorption of pyridine occurs (T_D), as indicated by the start of TPD chromatograms, and the temperature corresponding to the maximum of the TPD chromatogram (T_m) increases with the decrease in the value of θ_i.

The results, viz., the decrease in the chemisorption of pyridine with temperature (Fig. 2a), the increase in T_D or T_m with the decrease in the value of θ_i (Fig. 3), and the site energy distribution shown in Fig. 2b, reveal the presence of broad site energy distribution on the catalyst.

Influence of Poisoning

The results on the *o*-xylene isomerization and isooctane cracking reactions at 608 K over the catalyst (particle size: 0.018 cm) with and without poisoning by 4-methylquinoline [which poisons selectively the acid sites on the external surface of the crystals of ZSM-5 (*17, 18*) and hence expected to poison only the acid sites in the macro- and mesopores of the catalyst] and pyridine (which can penetrate the macro-, and meso-, and micropores of the catalyst) are presented in Tables 2 and 3, respectively.

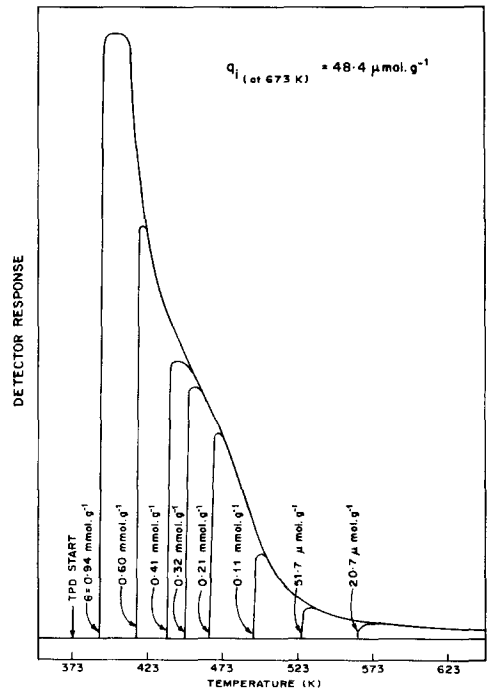

FIG. 3. TPD chromatograms of pyridine on the catalyst under chromatographic conditions (amount of catalyst, 0.30 g; He flow rate, 10 cm^3 · min^{-1}; heating rate, 10 K · min^{-1}).

TABLE 2

Data on the Activity and Product Distribution in the *o*-Xylene Isomerization at 608 K over the Catalyst (d_p = 0.018 cm) with and without Poisoning by 4-Methylquinoline and Pyridine

	Unpoisoned catalyst	Catalyst poisoned by 4-methylquinoline	Catalyst poisoned by pyridine
Conversion of *o*-xylene (%)	8.60	4.29	1.79
Hydrocarbon		Concentration (wt%)	
Aliphatics	0.05	0.07	0.03
Benzene	0.04	0.03	0.03
Toluene	0.11	0.13	0.12
p-Xylene	3.95	1.47	0.55
m-Xylene	4.45	2.59	1.07
o-Xylene	91.40	95.7	98.20
C_{9+} aromatics	—	0.01	—
Total	100	100	100
p-X/m-X ratio	0.89	0.56	0.50

Note. Reaction conditions: amount of catalyst, 0.1 g; H_2 flow rate, 104 $cm^3 \cdot min^{-1}$; pulse size, 1.4 μl; pressure, 205 kPa.

In case of the *o*-xylene isomerization, the catalytic activity and selectivity (for *p*-xylene) are decreased due to the poisoning of the catalyst with either of the two bases; the influence of poisoning by pyridine is, however, much more pronounced. It is interesting to note that the catalyst activity is reduced to its half-value because of the chemisorption of 4-methylquinoline in the macro- and mesopores.

In case of the cracking of isooctane, the catalyst poisoning by both the bases results in a drastic decrease in the activity of catalyst, and the decrease in the catalytic activity is almost the same. This fact indicates that the cracking of isooctane occurs essentially in the macro- and mesopores of the catalyst. This is consistent with the earlier observation that isooctane does not penetrate the channels of ZSM-5 (*9*).

Influence of Particle Size on Catalytic Activity and Selectivity

In order to find the influence of intercrystalline (macropore) mass transfer on the catalytic activity and selectivity (or product distribution) in the methanol-to-aromatics conversion, *o*-xylene isomerization, and isooctane cracking reactions on the catalyst, these reactions were carried out using the catalyst of different particle sizes.

The influence of catalyst particle size on the formation of aromatics and their distribution in the conversion of methanol on the catalyst at 673 K is shown in Table 4. It is very interesting to note that the aromatization in the methanol conversion is very strongly influenced by the catalyst particle size; the extent of aromatization is increased very significantly with the increase in the catalyst particle size. The distribution of aromatics formed in the methanol conversion reaction is also strongly influ-

TABLE 3

Data on the Cracking of Isooctane at 608 K on the Catalyst (d_p = 0.018 cm) with and without Poisoning by 4-Methylquinoline and Pyridine

Catalyst	Conversion (%)
Unpoisoned	17.9
Poisoned with 4-methylquinoline	1.30
Poisoned with pyridine	1.28

Note. Reaction conditions: amount of catalyst, 0.1 g; H_2 flow rate, 104 $cm^3 \cdot min^{-1}$; temperature, 608 K; pulse size, 3.0 μl; pressure, 205 kPa.

TABLE 4

Data on Activity and Product Distribution in the Methanol-to-Aromatics Conversion on the Catalyst of Different Particle Sizes

Particle size, d_p (cm)	0.16	0.04	0.018	0.16	0.04	0.018
Amount of catalyst (g)	0.20	0.20	0.20	0.02	0.02	0.02
Conversion of methanol (%)	100	100	100	96.4	96.9	97.2
Concentration of aromatics in hydrocarbons (%)	21.0	18.8	8.80	5.96	2.80	1.16
Distribution of aromatics (wt%)						
Benzene	2.10	5.00	5.68			
Toluene	9.14	17.1	15.7			
Ethylbenzene	2.86	2.90	4.89			
p-Xylene	16.9	15.4	16.4			
m-Xylene	19.0	17.3	16.7			
o-Xylene	15.0	13.7	13.4			
(Total xylenes)	(50.9)	(46.7)	(46.5)			
C_{9+} aromatics	35.0	28.3	27.3			
Total	100	100	100			
p-X/m-X	0.89	0.91	0.98			
p-X/o-X	1.12	1.15	1.22			

Note. Reaction conditions: temperature, 673 K, H_2 flow rate, 80 $cm^3 \cdot min^{-1}$; pulse size, 2.0 μl; pressure, 203 kPa.

enced by the catalyst particle size. The concentration of benzene, toluene, and ethylbenzene in the aromatics is decreased but that of xylenes and C_{9+} aromatics is increased with the increase in the catalyst particle size. It may also be noted that the selectivity of *p*-xylene formation (*p-X/m-X* or *p-X/o-X* ratio) is decreased with the increase in the particle size.

The results on the *o*-xylene isomerization at 673 K over the catalyst of different particle size are given in Table 5. The catalyst

TABLE 5

Data on Activity and Product Distribution in the *o*-Xylene Isomerization on the Catalyst of Different Particle Sizes

Particle size, d_p (cm)	0.16	0.04	0.018	0.16	0.04	0.018
Amount of catalyst (g)	0.20	0.20	0.20	0.02	0.02	0.02
Conversion of *o*-xylene (%)	31.4	36.4	38.0	4.9	5.2	6.3
Xylene loss (wt%)	1.7	1.4	0.9	1.2	0.8	0.7
Hydrocarbon			Concentration (wt%)			
Aliphatics	0.52	0.44	0.31	0.58	0.49	0.50
Benzene	0.08	0.07	0.05	0.11	0.02	0.01
Toluene	0.90	0.70	0.36	0.42	0.27	0.14
p-Xylene	13.8	15.9	16.6	1.95	2.38	3.01
m-Xylene	15.9	19.1	20.5	1.74	2.04	2.52
o-Xylene	68.6	63.6	62.0	95.1	94.8	93.7
C_{9+} aromatics	0.20	0.19	0.18	0.10	—	0.12
Total	100	100	100	100	100	100
p-X/m-X ratio	0.86	0.83	0.81	1.12	1.16	1.19

Note. Reaction conditions: temperature, 673 K, H_2 flow rate, 80 $cm^3 \cdot min^{-1}$; pulse size, 2.0 μl; pressure, 203 kPa.

TABLE 6

Results on the Isooctane Cracking at 673 K on the Catalyst of Different Particle Sizes

Particle size, d_p (cm)	0.16	0.04
Conversion of isooctane (%)	44.0	80.8
Selectivity for aromatics (%)	3.18	6.06
Hydrocarbon distribution	Concentration (wt%)	
Isooctane	56.0	19.2
Other aliphatics	42.6	75.9
Aromatics	1.40	4.90
Total	100	100

Note. Reaction conditions: amount of catalyst, 0.2 g; H_2 flow rate, 80 $cm^3 \cdot min^{-1}$; pulse size, 2.0 μl; pressure, 205 kPa.

activity (i.e., conversion of *o*-xylene) is decreased, the xylene loss in the reaction (resulted by the dealkylation and disproportionation reactions of xylene, occurring simultaneously with the isomerization reaction) is increased, and also the product distribution is significantly changed because of the increase in the catalyst particle size.

The data on the activity and selectivity in the isooctane cracking over the catalyst of different particle sizes are presented in Table 6. Both the isooctane cracking activity and the selectivity in the formation of aromatics on the catalyst are decreased to a larger extent with the increase in the catalyst particle size.

It may be noted that isooctane does not penetrate the zeolite channels but the primary products of isooctane cracking (i.e., isobutene and isobutane) can. The formation of aromatics is expected from the conversion of the cracking products in the zeolite channels.

Influence of Particle Size on Reaction Kinetics

The pulse microcatalytic reactor data on the conversion in the *o*-xylene isomerization and isooctane cracking reactions on the catalyst of different particle sizes (0.018–0.16 cm) at different temperatures and flow rates are given elsewhere (*19*). The data have been analyzed using the following rate equation for a first-order solid catalyzed reaction, when carried out by using the pulse microreactor technique (*16*),

$$\ln [1/(1 - x)] = k_a (273\ R \cdot W)\ (1/F^\circ) \quad (1)$$

$$F^0 = (273/T_f)F \quad (2)$$

and

$$k_a = k \cdot K, \quad (3)$$

where k_a is the apparent reaction rate constant; k, the surface reaction rate constant; K, the adsorption equilibrium constant; x, the fractional conversion; F, the carrier gas flow rate; W, the weight of catalyst; R, the gas constant; and T_f, the temperature at which the gas flow rate is measured.

The $\ln [1/(1 - x)]$ vs $1/F^0$ plots, according to Eq. (1), for the isomerization of *o*-xylene on the catalyst of different particle sizes and temperatures are shown in Fig. 4. The plots are linear and also pass through the origin indicating a good fit of the data to Eq. (1). It may be noted that at the highest tem-

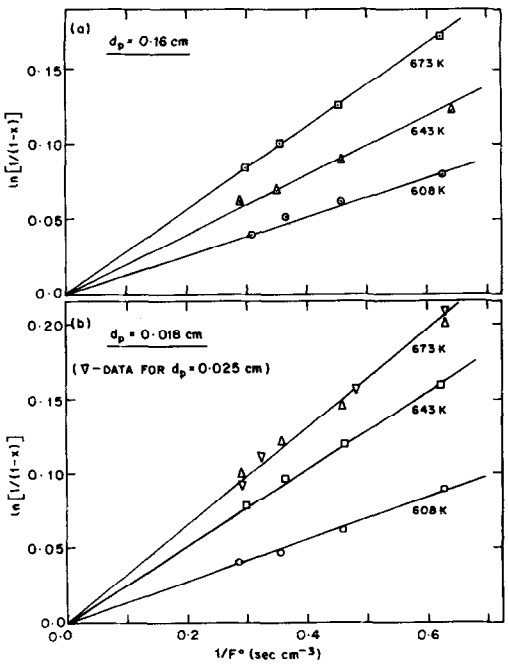

FIG. 4. First-order plots for the isomerization of *o*-xylene on the catalyst of different particle sizes.

TABLE 7

Apparent Reaction Rate Constants (k_a), Activation Energy [E_a], and Frequency Factor (A_a) for the *o*-Xylene Isomerization on the Catalyst of Different Particle Sizes

Catalyst particle size d_p (cm)	$k_a \times 10^5$ (mol · atm^{-1} · g^{-1} · sec^{-1})			E_a (kJ · mol^{-1})	A_a (mol · atm^{-1} · g^{-1} · sec^{-1})
	608 K	643 K	673 K		
0.16	5.76	8.75	12.3	37.74	0.10
0.025	—	—	14.6	—	—
0.018	6.19	11.4	14.6	46.08	0.55

perature of the study (i.e., 673 K), the data for the catalyst particle size, $d_p = 0.025$ and 0.018 cm, lie on the same plot (Fig. 4b). This indicates that the isomerization reaction is not influenced when the catalyst particle size is less than or equal to 0.025 cm.

The values of the apparent reaction rate constant (k_a) for the *o*-xylene isomerization, obtained from the slopes of the linear plots in Fig. 4, are given in Table 7.

The temperature dependence of k_a, for the isomerization on the catalyst of two particle sizes ($d_p = 0.018$ and 0.16 cm), according to the Arrhenius equation, is shown in Fig. 5. The values of apparent activation energy [E_a] and frequency factor (A_a) are included in Table 7. The results indicate that the increase in the catalyst particle size from 0.018 to 0.16 cm results in a significant decrease in the apparent reaction rate constant, activation energy, and frequency factor of the isomerization reaction.

The fact that isooctane does not penetrate the micropores of the zeolite crystallites even at 673 K has been utilized in the present study for measuring effective diffusivity in the intercrystalline and inter (alumina) particle pores (macropores) of the catalyst under reaction conditions/during catalysis, by investigating the cracking of isooctane on the catalyst of different particle sizes.

Figure 6 shows the linear ln [1/(1 − *x*)] vs $1/F^0$ plots, passing through origin, for the

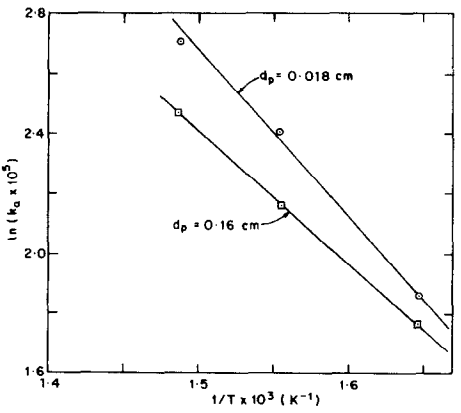

FIG. 5. Arrhenius plots for the isomerization of *o*-xylene on the catalyst of different particle sizes.

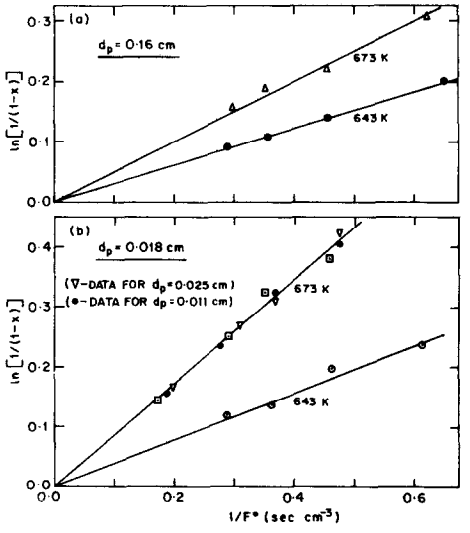

FIG. 6. First-order kinetic plots (according to Eq. (1)) for the cracking of isooctane on the catalyst of different particle sizes.

TABLE 8

Apparent Rate Constants (k_a) for the Isooctane Cracking on the Catalyst of Different Particle Sizes

Catalyst particle size d_p (cm)	$k_a \times 10^5$ (mol · atm^{-1} · g^{-1} · sec^{-1})	
	643 K	673 K
0.160	13.1	22.0
0.025	—	38.2
0.018	17.5	38.2

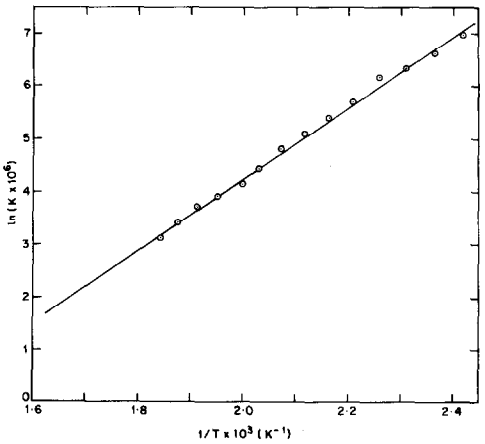

FIG. 7. Temperature dependence of adsorption equilibrium constant (K) for isooctane on the catalyst.

isooctane cracking on the catalyst of different particle sizes (0.018–0.16 cm) at two different temperatures (643 and 673 K). The values of the apparent reaction rate constant (k_a) for the cracking reaction are presented in Table 8. From the results (Fig. 6 and Table 8), it is clear that the reaction is not influenced by the catalyst particle size ≤0.025 cm. This leads to the conclusion that the reaction on the catalyst of particle size of 0.018 cm at 673 K is not influenced by the intraparticle (i.e., macropore diffusional) mass transfer and also not affected by the external (film diffusional) mass transfer. The rate parameter for the reaction, obtained at the above conditions, is therefore intrinsic (i.e., uncontaminated by the mass transfer effects).

The adsorption equilibrium constant (K) for isooctane on the catalyst at different temperatures (413–543 K) has been determined from its retention volumes measured by the GC pulse technique, using the relation (*16*)

$$K = V_R/RT_c, \qquad (4)$$

where V_R is the corrected retention volume and T_c the column (or catalyst) temperature. The temperature dependence of K, according to the van't Hoff equation is shown in Fig. 7. The value of heat of adsorption of isooctane on the catalyst (estimated from the slope of the linear ln K vs $1/T$ plot in Fig. 7) is found to be 56.1 kJ · mol^{-1}.

The values of K at 643 and 673 K were obtained from the extrapolation of the ln K vs $1/T$ plot, which is expected to be linear for a wide temperature range. The direct determination of K from the measurement of retention volume data at these temperatures was not possible because the adsorbate (i.e., isooctane) was found to undergo extensive reaction on the catalyst at higher temperatures (≥573 K).

The values of k for the isooctane cracking obtained from Eq. (3) are given in Table 9. The values of activation energy and frequency factor for the reaction on the catalyst of two different particle sizes are also presented in Table 9. The data show that the increase in the particle size from 0.018 to 0.16 cm causes a very significant de-

TABLE 9

Data on Surface Reaction Rate Constant (k), Activation Energy (E), and Frequency Factor (A) for the Isooctane Cracking on the Catalyst of Different Particle Sizes

Catalyst particle size d_p (cm)	k (sec^{-1})		E (kJ · mol^{-1})	A (sec^{-1})
	643 K	673 K		
0.160	35.0	96.4	121.5	2.6×10^{11}
0.026	—	167.4	—	—
0.018	47.2	167.4	151.8	1.02×10^{14}
0.011	—	167.4	—	—

TABLE 10

Catalyst Effectiveness Factors (η) and Thiele Modulus (ϕ_s) for the Isooctane Cracking on the Catalyst of Different Particle Sizes

Catalyst particle size d_p (cm)	η		ϕ_s	
	643 K	673 K	643 K	673 K
0.160	0.74	0.58	2.50	3.79
0.026	—	1.0	—	—
0.018	1.0	1.0	—	—
0.011	—	1.0	—	—

crease in the surface reaction rate constant and activation energy of the reaction. The reaction mechanism is shifted from chemical control to intraparticle mass transfer control with the increase in the catalyst particle size.

The values of catalyst effectiveness factors (η), which are defined as

$$\eta = k/k(\text{intrinsic}), \qquad (5)$$

where k(intrinsic) is the intrinsic surface reaction rate constant [i.e., k obtained in the absence of any mass transfer resistance], and Thiele modulus (ϕ_s), obtained from the η vs ϕ_s plot for the first-order reaction (*20*) for the catalyst of different particle sizes at 643 and 673 K, are given in Table 10.

The effective diffusion coefficient (D_e) for isooctane in the macropores of the catalyst is estimated using the relation (*20*)

$$\sigma_s = R\sqrt{k/D_e}, \qquad (6)$$

where ϕ_s is the Thiele modulus; R, the radius of catalyst particle; k, the intrinsic reaction rate constant; and D_e, the effective diffusion coefficient. The values of D_e at two different temperatures are given in Table 11.

DISCUSSION

Pore Systems in the Catalyst

The catalyst, which is in the form of extrudates, contains crystallites (0.2–0.3 μm) of the zeolite and particles of high surface area (about 200 $m^2 \cdot g^{-1}$) alumina. It is, therefore, expected to contain three distinct pore systems: (i) the intracrystalline pores (micropores of diam $\simeq$0.6 nm) of the zeolite, (ii) the intraparticle pores in the alumina particles (mesopores), and (iii) the intercrystalline and interalumina particles pores (macropores). The nonzeolitic pores of the catalyst (which comprises the intraparticle pores in the alumina and the interparticle and intercrystalline pores) are expected to have a bimodal pore size distribution as shown in Fig. 1. The mesopores ($r_p < 170$ nm, r_p (average) $\simeq$7.0 nm) are expected to be present in the fine particles of alumina. Whereas, the macropores are expected to be the voids in the zeolite crystallites and the alumina particles in the extrudates of the catalyst.

The total volume of the macro- and mesopores determined by specific gravity bottle method (i.e., 0.57 $cm^3 \cdot g^{-1}$) is in a good agreement with the one [>0.53 $cm^3 \cdot g^{-1}$, as even at the pressure of 33,000 psig, the pore volume vs pressure curve shows an increasing trend, as shown in Fig. 1] obtained by the mercury porosimetry.

It may be noted that the change in the catalyst particle size is not expected to effect the resistance to mass transfer (if present) in the mesopores or in the pores of the alumina particles. The observed influence of the catalyst particle size on the catalytic reaction is, therefore, a consequence of the change in the resistance to mass transfer in the intercrystalline and inter-

TABLE 11

Data on Macropore Effective Diffusivity (D_e), Bulk (Binary) Diffusion Coefficient ($D_{1,2}$) for Isooctane–H_2 System and Tortuosity Factor (τ) of the Catalyst for the Diffusion of Isooctane in Macropores of the Catalyst (Catalyst Particle Size, d_p = 0.16 cm)

Temperature (K)	Mean free path[a] λ (nm)	D_e ($cm^2 \cdot sec^{-1}$)	$D_{1,2}$[b] ($cm^2 \cdot sec^{-1}$)	τ
643	25.6	0.048	0.52	1.73
673	26.6	0.075	0.56	1.20

[a] Obtained from the relation given elsewhere (*25*).
[b] Estimated from the expression given by Fuller *et al.* (*26*).

(alumina) particle pores (i.e., in the macropores).

Poisoning of Inter- and Intracrystalline Acid Sites

The intercrystalline acid sites, which also include the intra- and interparticle sites on the alumina, are selectively blocked by the chemisorbed 4-methylquinoline, whereas the acid sites in the micro- macro-, and mesopores of the catalyst were poisoned by the chemisorption of pyridine.

The 4-methylquinoline poisoning has resulted in a very significant decrease in the *o*-xylene isomerization activity of the catalyst (Table 2). The decrease in the catalytic activity is expected for two reasons: first, because of poisoning of the intercrystalline acid sites involved in the catalytic reaction, and second, because of the chemisorption of the large molecular size base at or near the entrance of the zeolite channels (i.e., by pore mouth blocking/poisoning), thereby strongly influencing the diffusion of *o*-xylene in the zeolite. The second reason seems to be the most probable one, as it is consistent with the observation made in the *p*-xylene isomerization on H–ZSM-5 by Namba *et al.* (*21*).

In the isooctane cracking, the poisoning by both the bases results in a drastic decrease in the catalytic activity and the decrease in both the cases is the same. This observation is consistent with the fact that isooctane does not penetrate the micropores of the zeolite.

Influence of Intercrystalline Mass Transfer

For the zeolite catalyst, the diffusion path and, consequently, the intercrystalline mass transfer resistance are increased with the increase in catalyst particle size. The results (Tables 4–6) reveal that the catalytic activity and selectivity (or product distribution) in the reactions (viz. *o*-xylene isomerization, methanol-to-aromatics conversion, and conversion of the primary products of isooctane cracking to aromatics) occurring almost solely in the micropores or channels of the zeolite are strongly influenced by the catalyst particle size and, hence, by the intercrystalline mass transfer, as discussed below.

The formation of aromatics in the methanol conversion is very much favored on the catalyst of larger and larger particle size (Table 4). The increase in the extent of aromatization with the increase in the catalyst particle size is consistent with the observation made earlier by Riekert and co-workers (*6*, *7*) in the conversion of dimethyl ether on H–ZSM-5.

It is interesting to note that not only the extent of aromatization but also the distribution of aromatics is influenced by the catalyst particle size. This influence can be explained as follows.

The conversion of methanol-to-hydrocarbons on ZSM-5 zeolite can be represented by the following simplified reaction scheme (*7*, *22*):

$$CH_3OH \rightleftarrows (CH_3)_2O \rightarrow C_2\text{–}C_5 \text{ olefins} \rightarrow \begin{matrix} \text{aromatic} + \text{paraffins} \\ \downarrow \\ \text{alkylated aromatics} \end{matrix}$$

The aromatics, which are the end products, are formed in the consecutive reaction involving a number of steps. The formation of thermodynamically stable end products in such a consecutive reaction is always favored in the presence of mass transfer resistance (i.e., when the reaction is controlled by mass transfer) (*20*). It may also be noted that since the hydrocarbon formation from methanol is an exothermic reaction (*1*), for the catalyst of larger particle size, the temperature at the center of the catalyst particle is expected to be higher than that at the surface of the particle. The occurrence of the methanol conversion reaction at the temperature higher than that actually measured is also expected to be responsible to some extent for the higher formation of aromatics on the larger particle size catalyst. [The formation of aromatics in methanol conversion on H–ZSM-5 in

a pulse microreactor was found to increase with the increase in temperature from 648 to 773 K (*23*).]

The distribution of aromatics in alcohol conversion on H–ZSM-5 is controlled mostly by the reactions of aromatic hydrocarbons, in particularly, by the isomerization and dealkylation reactions (*23, 24*). The increase in the concentration of higher alkylbenzenes (C_{9+} aromatics) and the decrease in the concentration of benzene and toluene in the aromatics with the increase in catalyst particle size (Table 4) are expected to be mostly due to the alkylation of benzene and toluene with methanol and/or lower olefins, under the condition of intercrystalline mass transfer control.

The *o*-xylene isomerization activity and selectivity of the catalyst is also affected significantly by the intercrystalline mass transfer. The formation of C_{9+} aromatics in xylene disproportionation and alkylation reactions is affected only to a small extent. However, the very significant increase in the formation of benzene and toluene with the increase in the catalyst particle size indicates that the dealkylation of xylenes is favored under the conditions of intercrystalline mass transfer control. Thus the xylene loss is increased with the increase in the intercrystalline mass transfer resistance.

The results on the kinetics of the *o*-xylene isomerization over the catalyst of different particle sizes (Table 7) reveal that, for the catalyst particles ≤ 0.025 cm, the reaction is not influenced by the intercrystalline mass transfer. However, when the catalyst particle size is increased to 0.16 cm, the reaction rate is influenced by the intercrystalline mass transfer and, consequently, the apparent activation energy for the reaction is decreased considerably [from 46.08 kJ · mol^{-1} (for $d_p = 0.018$ cm) to 37.74 kJ · mol^{-1} (for $d_p = 0.16$ cm)].

The fact that isooctane cannot penetrate the intracrystalline (micro) pores of the catalyst, has made it possible to determine the effective intercrystalline or macropore diffusivity of the catalyst by studying the cracking of isooctane on the catalyst of different particle sizes. The effective diffusivity was estimated from the knowledge of the Thiele modulus (obtained from experimentally measured catalyst effectiveness factor) and the intrinsic surface reaction rate constant (obtained experimentally using the catalyst of a very small particle size). It may be noted that the increase in the catalyst particle size results in the increase in the resistance for the mass transfer in the macropores (i.e., intercrystalline and interalumina particle pores). Therefore, the effective diffusivity, thus measured, corresponds to the macropore effective diffusivity of the catalyst. Also, since the alumina particles (which contain the mesopores) used in the catalyst are very fine, the lengths of mesopores in the alumina particles are short and, therefore, their effectiveness factor, $\eta_{(meso)}$, is expected to be essentially unity (*20*). Hence, the rate of isooctane cracking on the catalyst of particle size 0.16 cm at 643 and 673 K is controlled essentially by the macropore diffusion.

The mean free path of the isooctane molecules at 643 and 673 K (Table 11) is much smaller than the macropore size (average macropore diam: $\simeq 0.2$ μm). The diffusion of isooctane in the macropores is, therefore, expected to be due to the bulk diffusion. The tortuosity factor of the catalyst for the diffusion in the macropores could be estimated from the knowledge of the effective diffusivity (D_e), the bulk diffusion coefficient ($D_{1,2}$) for the isooctane–H_2 system, and the macroporosity [$\varepsilon_{(macro)}$] of the catalyst using the relation

$$D_e = D_{1,2}\, \varepsilon_{(macro)}/\tau. \qquad (7)$$

The values of τ are included in Table 11. The values of τ are different at the two temperatures and also are lower than the theoretical value of $\tau = 3$ (*27, 28*). These facts indicate the possibility of the intraparticle diffusion being influenced by adsorption and/or surface diffusion of isooctane.

Generally, the diffusion in porous catalysts and adsorbents is retarded because of adsorption of the diffusion species on the pore walls, whereas, it is enhanced due to surface diffusion of the adsorbed species, which is an activated process. The influence of adsorption and surface diffusion on the effective diffusivity and, consequently, on the estimated τ is expected to be dependent upon the temperature; the diffusion is retarded at lower temperatures, while it is enhanced at higher temperatures. The decrease in τ with the increase in the temperature (Table 11) is consistent with the fact that the diffusion is enhanced due to the decrease in the adsorption of diffusing species and also by the increase in the surface mobility fo the adsorbed species.

The effective diffusivity of isooctane in the catalyst at 423 K under nonreacting conditions, measured using the GC pulse technique based on pulse broading and evaluating the diffusivity from the expression derived by Grubner (*29*), is found to be 0.0031 $cm^2 \cdot sec^{-1}$ (*30*). This value is much lower than that obtained in the present study (Table 11). This is mostly for two reasons—first, due to the retardation of the diffusion because of higher adsorption of isooctane on the catalyst at the lower temperature and second, the diffusivity measured by the GC pulse technique under nonreacting conditions is due to the contribution of the diffusion in both macro- and mesopores of the catalyst involving bulk and Knudson diffusion, respectively.

CONCLUSIONS

Both the catalytic activity and the selectivity (or product distribution) in the methanol-to-aromatics conversion and *o*-xylene isomerization over ZSM-5 zeolite are strongly influenced by the intercrystalline mass transfer, particularly when the catalyst (containing the zeolite) of large particle size is used. When the intercrystalline mass transfer resistance is increased by increasing the catalyst particle size, the following observations on the selectivity in the above reactions are made: The extent of aromatization in the methanol conversion is drastically increased and the formation of higher or polyalkylbenzenes is also favored over that of benzene and toluene. The xylene loss in the *o*-xylene isomerization, resulting from the dealkylation and disproportionation of xylenes, is increased significantly.

The effective intercrystalline pore diffusivity of the catalyst containing ZSM-5 zeolite could be conveniently measured under reaction conditions by studying the cracking of isooctane on the catalyst of different particle sizes. The effective intercrystalline pore diffusivity of the catalyst for isooctane has been found to be 0.048 $cm^2 \cdot sec^{-1}$ at 643 K and 0.075 $cm^2 \cdot sec^{-1}$ at 673 K. The tortuosity factor of the catalyst for the diffusion in the macropores has been estimated to be 1.73 at 648 K and 1.2 at 673 K.

ACKNOWLEDGMENT

The authors are grateful to Dr. P. Ratnasamy (National Chemical Laboratory, Pune) for providing the catalyst.

REFERENCES

1. Chang, C. D., *Catal. Rev. Sci. Eng.* **25,** 1 (1983).
2. Chang, C. D., *Catal. Rev. Sci. Eng.* **26,** 323 (1984). Chang, C. D., "Hydrocarbons from Methanol." Dekker, New York, 1983.
3. Scott, J. (Ed.), "Zeolite Technology and Applications—Recent Advances." Noyes Data Corp., Park Ridge, NJ 1980.
4. Kaeding, W. W., Barik, G. C., and Wu, M. M., *Catal. Rev. Sci. Eng.* **26,** 597 (1984).
5. Palekar, M. G., and Rajadhyaksha, R. A., *Catal. Rev. Sci. Eng.* **28,** 371 (1986).
6. Doelle, H. J., Heering, J., Riekert, L., and Marosi, L., *J. Catal.* **71,** 27 (1980).
7. Heering, J., Kotter, M., and Riekert, L., *Chem. Eng. Sci.* **37,** 581 (1982).
8. Choudhary, V. R., and Vaidya, S. H., *Res. Ind.* **26,** 1 (1981).
9. Choudhary, V. R., and Singh, A. P., *Zeolites* **6,** 206 (1986).
10. Gregg, S. J., and Sing, K. S. W., "Adsorption Surface Area and Porosity." Academic Press, London, 1967.
11. Choudhary, V. R., *J. Chromatogr.* **259,** 283 (1983).
12. Choudhary, V. R., and Nayak, V. S., *Appl. Catal.* **4,** 31 (1982).
13. Nayak, V. S., and Choudhary, V. R., *Appl. Catal.* **4,** 333 (1982).

14. Nayak, V. S., and Choudhary, V. R., *J. Catal.* **81,** 26 (1983).
15. Choudhary, V. R., *Zeolites* **7,** 272 (1987).
16. Bassett, D. W., and Habgood, H. W., *J. Phys. Chem.* **64,** 760 (1960).
17. Anderson, J. A., Foger, K., Mole, T., Rajadhyaksha, R. A., and Sanders, J. V., *J. Catal.* **58,** 114 (1979).
18. Yashima, T., Sakaguchi, Y., and Namba, S., *Stud. Surf. Sci. Catal.* **7,** 739 (1981).
19. Akolekar, D. B., Ph.D. thesis, Univ. of Poona, 1987.
20. Satterfield, C. N., "Mass Transfer in Heterogeneous Catalysis." M.I.T. Press, Cambridge, MA 1970.
21. Namba, S., Nakanishi, S., and Yashima, T., *J. Catal.* **88,** 505 (1984).
22. Chang, C. D., *Chem. Eng. Sci.* **35,** 619 (1980).
23. Choudhary, V. R., and Sansare, S. D., *Indian J. Technol.* **23,** 326 (1985).
24. Choudhary, V. R., and Sansare, S. D., *Appl. Catal.* **10,** 147 (1984).
25. Maron, S. H., and Prutton, C. F., "Principles of Physical Chemistry," p. 26. MacMillan Co., New York, 1959.
26. Fuller, E. N., Schettler, P. D., and Giddings, J. C., *Ind. Eng. Chem.* **58,** 19 (1966).
27. Johnson, M. F. L., and Stewart, W. E., *J. Catal.* **4,** 248 (1965).
28. Feng, C., and Stewart, W. E., *Ind. Eng. Chem. Fundam.* **12,** 143 (1973).
29. Grubner, O., *Adv. Chromatogr.* **6,** 173 (1968).
30. Choudhary, V. R., Mayadevi, S., and Akolekar, D. B., unpublished work.